Geochimica et Cosmochimica Acta, Vol. 69, No. 1, pp. 177-188, 2005

0016-7037/05 $30.00 + .00

doi:10.1016/j.gca.2004.06.017

Supernova graphite in the NanoSIMS: Carbon, oxygen and titanium isotopic compositions of a spherule and its TiC sub-components

F. J. Stadermann,* T. K. Croat, T. J. Bernatowicz, S. Amari, S. Messenger,† R. M. Walker‡ and E. Zinner
Laboratory for Space Sciences and Physics Department, Washington University, St. Louis, MO 63130-4899, USA

(*Received December* 17, 2003; *accepted in revised form June* 14, 2004)

Abstract—Presolar graphite spherules from the Murchison low-density separate KE3 contain a large number of internal TiC crystals that range in size from 15 to 500 nm. We have studied one such graphite grain in great detail by successive analyses with SEM, ims3f SIMS, TEM and NanoSIMS. Isotopic measurements of the 'bulk' particle in the ims3f indicate a supernova origin for this graphite spherule. The NanoSIMS measurements of C, N, O and Ti isotopes were performed directly on TEM ultramicrotome sections of the spherule, allowing correlated studies of the isotopic and mineralogical properties of the graphite grain and its internal crystals. We found isotopic gradients in $^{12}C/^{13}C$ and $^{16}O/^{18}O$ from the core of the graphite spherule to its perimeter, with the most anomalous compositions being present in the center. These gradients may be the result of isotopic exchange with isotopically normal material, either in the laboratory or during the particle's history. No similar isotopic gradients were found in the $^{16}O/^{17}O$ and $^{14}N/^{15}N$ ratios, which are normal within analytical uncertainty throughout the graphite spherule. Due to an unusually high O signal, internal TiC crystals were easily located during NanoSIMS imaging measurements. It was thus possible to determine isotopic compositions of several internal TiC grains independent of the surrounding graphite matrix. These TiC crystals are significantly more anomalous in their O isotopes than the graphite, with $^{16}O/^{18}O$ ratios ranging from 14 to 250 (compared to a terrestrial value of 499). Even the most centrally located TiC grains show significant variations in their O isotopic compositions from crystal to crystal. Measurement of the Ti isotopes in three TiC grains found no variations among them and no large differences between the compositions of the different crystals and the 'bulk' graphite spherule. However, the same three TiC crystals vary by a factor of 3 in their $^{16}O/^{18}O$ ratios. It is not clear in what form the O is associated with the TiC grains and whether it is cogenetic or the result of surface reactions on the TiC grains before they accreted onto the growing graphite spherule. The presence of ^{44}Ca from short-lived ^{44}Ti ($t_{1/2}$ = 60y) in one of the TiC subgrains confirms the identification of this graphite spherule as a supernova condensate. *Copyright © 2005 Elsevier Ltd*

1. INTRODUCTION

Several types of presolar grains with large isotopic anomalies have been identified in primitive meteorites in recent years. These grains predate the formation of the solar system materials into which they were incorporated, without completely losing their isotopic and mineralogical identities (e.g., articles in Bernatowicz and Zinner, 1997). The study of the preserved memory of their stellar origins allows identification of the stellar processes that led to their formation and of the physical and chemical conditions during their condensation (e.g., Huss and Lewis, 1995; Nittler, 2003). Laboratory studies of presolar grains have thereby contributed to our knowledge of nucleosynthesis and stellar evolution, as well as dust formation in stellar environments (e.g., Zinner, 1997; 1998).

One class of presolar grains is low-density (~1.7 g/cm^3) graphite spherules (Amari et al., 1994). These particles can be relatively large (up to 20 μm, Amari et al., 1995) and typically have high trace element concentrations (Hoppe et al., 1995), which makes it possible to measure the isotopic compositions of a large number of elements (Amari et al., 1995; Travaglio et al., 1999). Secondary ion mass spectrometry (SIMS) studies of individual low density graphite spheres have revealed considerable variations in C isotopic compositions (Amari et al., 1990; Hoppe et al., 1995), as well as large ^{18}O excesses (Amari et al., 1995), indicating a massive-star origin. A supernova origin for these particles was proven by the presence of ^{28}Si excesses and the inferred initial presence of extinct ^{41}Ca and ^{44}Ti (Amari et al., 1996; Nittler et al., 1996). Calculations based on supernova models (Woosley and Weaver, 1995) show that most of the isotopic signatures of low-density graphite spheres can be explained by mixing of different supernova zones (Travaglio et al., 1999). Studies of the internal structure of presolar graphite spherules in the TEM (transmission electron microscope) led to the discovery of presolar grains within presolar grains in the form of internal TiC crystals (Bernatowicz et al., 1991; 1996), and a recent TEM study of graphite spherules from supernovae determined the physical and chemical properties of these TiC subgrains (Croat et al., 2003). In this study, we take advantage of the high spatial resolution of the NanoSIMS to connect the microstructural and isotopic studies of presolar graphite spherules by making isotopic measurements of a graphite spherule and its subcomponents on the *same* ultramicrotome sections that were studied in the TEM.

2. EXPERIMENTAL

All NanoSIMS measurements were made on the presolar graphite spherule KE3e#10 (Croat et al., 2003) from the Murchison (CM2) density separate KE3, which consists of particles in the density range 1.65–1.72 g/cm^3 that are larger than 2 μm (Amari et al., 1995). This 12 μm diameter spherule was first deposited on high-purity Au foil for

* Author to whom correspondence should be addressed (fjs@wustl.edu).
† *Present address:* NASA JSC Code SR, Houston, Texas, USA.
‡ Deceased

morphologic and isotopic characterization in a JEOL JSM-840A scanning electron microscope and a CAMECA ims3f ion microprobe. Isotopic measurements of C, O, Mg/Al, Si and Ti indicate a supernova (SN) origin for KE3e#10 (Travaglio et al., 1999) and although all of these measurements were done sequentially with a destructive analysis technique (i.e., SIMS), less than 25% of the sample material was consumed in this step. It should be noted that these initial isotopic measurements with the ims3f instrument are referred to as 'bulk' measurements (as opposed to the later NanoSIMS measurements) although they sampled only part of the grain's volume.

After the initial isotopic characterization, the remainder of the spherule was removed from the Au foil, embedded in resin and then sliced with a diamond ultramicrotome (Reichert-Jung Ultracut E) into 70 nm thin sections. The sections were retrieved onto holey carbon film covered TEM grids for mineralogical studies. A total of 37 sections of KE3e#10 were analyzed in a 200 keV JEOL 2000-FX TEM, revealing abundant internal TiC crystals. These TiC subgrains range in size from 15 to 500 nm and constitute 1000 ppm of the spherule by volume. Textural and compositional evidence indicates that the TiC grains formed earlier than the graphite into which they were incorporated during its growth (Croat et al., 2003).

Following comprehensive TEM analyses, selected slices were analyzed in a CAMECA NanoSIMS, a new generation ion microprobe (Hillion et al., 1999), the first of which has been installed at Washington University in St. Louis (Stadermann et al., 1999). This instrument has high spatial resolution (Cs^+ beam diameter as small as 50 nm), high sensitivity at high mass resolution (up to 50 times higher than the ims3f ion microprobe) and parallel secondary ion detection with 6 electron multipliers and 1 Faraday cup, which make it ideally suited for the isotopic study of submicrometer phases. To prepare samples for the NanoSIMS, five TEM grids (each containing several sections of graphite particle KE3e#10) were placed on flat sample substrates and glued down by carefully applying a thin layer of carbon paint along the perimeter. These five grids contained a total of 11 sections, all of which were studied with the NanoSIMS, whereas only 9 were accessible to TEM measurements. This results from the fact that two of the ultramicrotome sections were located directly on top of the copper bars of the grid and were thus not visible in the TEM. Such sections can, however, be measured with a surface analysis technique like SIMS. In fact, due to the increased sample support, these samples are easier to study with SIMS than those suspended on the carbon film, although in these cases it is not possible to directly correlate mineralogical and isotopic data.

The NanoSIMS measurements of C, N and O isotopes were performed in imaging mode where a 50–100 nm Cs^+ primary ion beam of around 1 pA was rastered over a sample area of $10 \times 10\ \mu m^2$ to $20 \times 20\ \mu m^2$ while secondary electrons (SE) and negative secondary ion species were collected. Electron multipliers were used for the parallel detection of [$^{12}C^-$, $^{13}C^-$, $^{12}C^{14}N^-$, $^{12}C^{15}N^-$] for C-N and [$^{12}C^-$, $^{13}C^-$, $^{16}O^-$, $^{17}O^-$, $^{18}O^-$] for C-O isotopic measurements, respectively. Combined C-Si isotopic measurements were also attempted, but the Si signal was extremely low and no meaningful results were obtained. All images were acquired in 256^2 or 512^2 pixels and consisted of 10–40 repeated frames or layers per image. The term 'layers' is used to reflect the fact that the SIMS measurement slowly consumes the graphite section while sampling increasingly deeper regions. Under typical analysis conditions, the measurement of each layer consumes no more than a few nm of sample material. The acquisition time per layer varied between 2 and 30 min, resulting in measurement times of up to 20 hours for a single imaging analysis. All measurements were performed at the high mass resolution necessary to separate isobaric interferences (e.g., $^{16}O^1H$ or $^{11}B^{16}O$) from the signal of interest (e.g., ^{17}O or $^{12}C^{15}N$, respectively). The positions of all mass peaks were routinely checked before and after each measurement on standard particles. Since the images were acquired in multi-collection mode, the magnetic field remained static during the entire analysis. The stability of the mass spectrometer was guaranteed by the use of an NMR probe combined with precise temperature control, and variations of the magnetic field were found to be generally below 10 ppm. The primary ion beam current did occasionally vary by a few percent over the course of a long measurement, resulting in slightly changing secondary ion signals. However, such variations do not lead to isotopic artifacts because all species are measured simultaneously. In some imaging measurements we found evidence for small sample drift during the measurements (up to a few micrometers total displacement). Imaging artifacts created by this sample shift were corrected for during data processing, as described below.

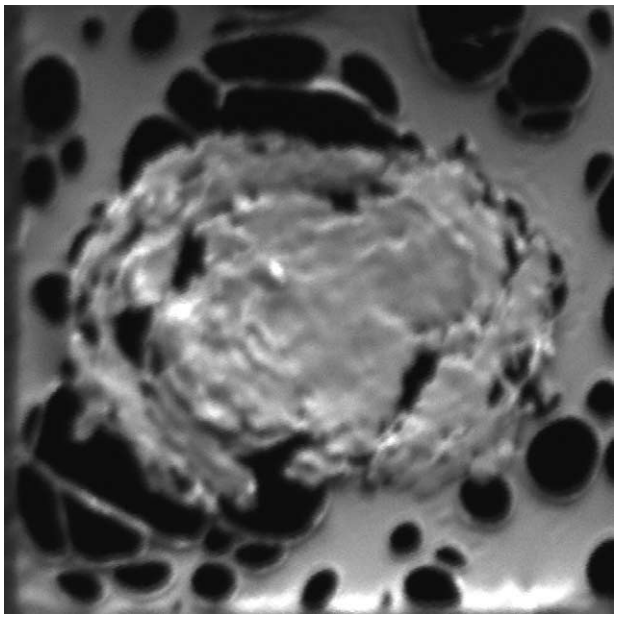

Fig. 1. Unsmoothed (raw) NanoSIMS secondary electron image of a TEM slice of presolar graphite grain KE3e#10. The area shown is $12 \times 12\ \mu m^2$, represented in 256×256 pixels, and the diameter of this off-center grain slice is roughly 9 μm. Secondary electron images can be acquired in parallel with negative secondary ion images in the NanoSIMS and the spatial resolution (which only depends on the primary ion beam diameter) is identical for both. This image was acquired halfway through an imaging run and one can see the growing holes in the supporting carbon film around the sample slice.

During SIMS analyses, sample material is slowly eroded (sputtered away) and a long imaging acquisition time results in the creation of a rectangular crater in the sample. The rectangular analysis area is chosen large enough to encompass the entire graphite section and some of the immediately surrounding TEM film that is used as internal isotopic standard (see below). In the case of TEM sections, the sample is only supported by the carbon film and the thin slice of embedding resin (Fig. 1), which are gradually destroyed during the course of a measurement. Since the sputter rates of the carbon film and the resin are significantly higher than that of the graphite sample, the sample support fails before the graphite itself is completely consumed (Fig. 2). In most cases, the sample support develops holes, which grow until the sample is only supported by a lacey net of carbon film remnants, which eventually breaks (Fig. 3). We estimate that at this point only roughly 1/3 of the sample volume has actually been consumed in the analysis. In sections that are lying on top of a copper bar of the TEM grid, the entire sample volume is available for the SIMS analysis.

Data are processed using custom software to correct for random outliers and possible stage drift, both which are generally small effects. It is not necessary to correct for image shifts of one ion species relative to another, because all species are measured simultaneously in multi-collection mode in the NanoSIMS. Typically, the first few layers of a measurement, which are dominated by isotopically normal surface contaminants, and the last layers, if the sample support fails, are eliminated. Shift-corrected images from the remaining layers are then added for each measured species to increase the total signal in the images.

Isotope ratio images are obtained by dividing the images of two species (e.g., ^{12}C and ^{13}C) pixel by pixel. Often it is necessary to smooth the images and to mask areas with low count rates from which no statistically meaningful ratios can be obtained. Isotopic anomalies

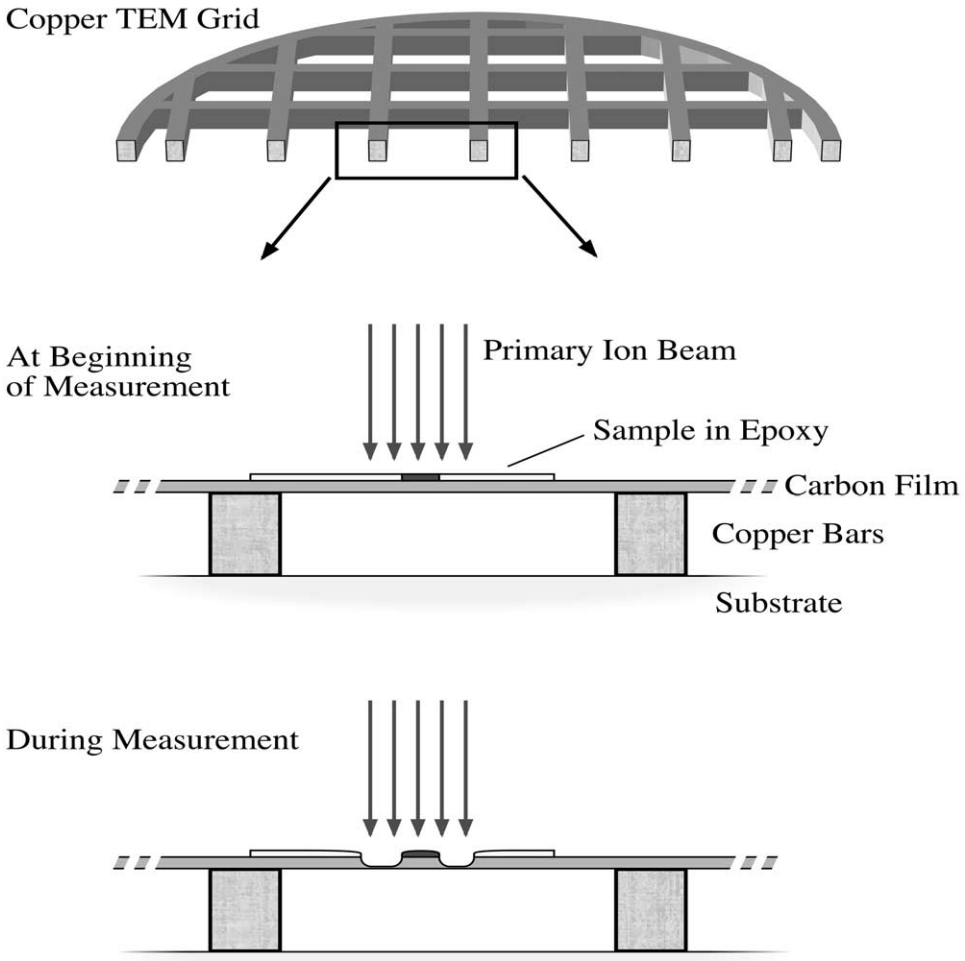

Fig. 2. Schematic of an ultramicrotome section on a carbon film covered TEM grid during NanoSIMS analysis. The bottom two images show a side view of a TEM grid detail at the beginning and during the analysis. The raster area of the primary beam overlaps the sample and erodes the supporting film, which has a higher sputter rate than the graphite grain section. After several hours of sputtering, all sample support is gone and the sample is lost, although only a fraction of the actual sample has been consumed in the measurement (cf. Fig. 3).

can also be verified by their presence throughout the individual layers of an imaging measurement, i.e., in a depth profile. This ensures that anomalous compositions seen in the ratio images are not due to a random fluctuation or an artifact within a single layer of the measurement. Measured ratios are calibrated to a standard of known isotopic composition. For the imaging measurements in this study the sample-supporting carbon film was used as an internal standard, because its C, N and O isotopic compositions can safely be assumed to be 'normal' within the precision of the measurements. In all C, N and O measurements the imaged areas covered the whole graphite grain slice and a rim of surrounding carbon film (see, e.g., Fig. 1), ensuring that sample and standard were present within the same image. The imaging results were not corrected for electron multiplier deadtime effects, because the count rates for all species rarely exceeded 10^5 s^{-1}, and for these measurements counting-statistical errors were much larger than deadtime effects.

A different analytical approach was used for the analysis of Ti isotopes in three individual TiC crystals. These measurements were made with an O^- primary beam and positive secondary ions. In the NanoSIMS the spatial resolution of the O^- beam is generally worse than that of the Cs^+ beam and primary beam tune-up for O^- is more difficult. In this case, however, the spatial resolution is not critical because virtually all Ti in these sections is contained in the TiC subgrains. Sample navigation on a scale below the resolution of the optical camera was done using the (non-mass-filtered) total secondary ion signal (Fig. 4). Most of this secondary ion signal comes from previously implanted Cs, which is extracted as Cs^+.

Although the NanoSIMS has six electron multipliers for the parallel detection of different masses, adjacent masses (i.e., $\Delta m = 1$ amu) can be measured in multicollection mode only up to mass 30 (e.g., ^{28}Si, ^{29}Si, ^{30}Si), due to the finite size of the electron multipliers. Therefore, to measure all 5 Ti isotopes (^{46}Ti to ^{50}Ti), a combined analysis mode (in which multicollection is combined with magnetic peak jumping) must be used. Thus, the Ti isotopes at odd and even masses are measured in separate steps by cycling the mass spectrometer through two different magnetic field values. Since not all detectors are needed for the Ti isotopes in this setup, we also measured several Ca isotopes. In step one ^{40}Ca, ^{43}Ca, ^{46}Ti, ^{48}Ti, and ^{50}Ti were measured in electron multipliers 1–5 and in step two ^{44}Ca, ^{47}Ti, and ^{49}Ti in detectors 2, 3, and 4. Measurements are done at high mass resolution and although ^{48}Ca could not be separated from ^{48}Ti, the inferred contribution from ^{48}Ca was so low that it could safely be neglected. Corrections for possible interferences from ^{50}Cr (Hoppe and Besmehn, 2002) were not required due to the low Cr content in the TiC grains (average Cr/Ti ratio of 0.003). A perovskite ($CaTiO_3$) standard was used for tune-up and external calibration of the isotopic ratios for instrumental mass fractionation and multicollection detector differences. After a TiC crystal was located by Ti elemental imaging in 256 × 256 pixel (Fig. 5), the primary ion beam was rastered over a small (5 × 5 pixel) area for the combined analysis mode measurement. The isotopic ratios

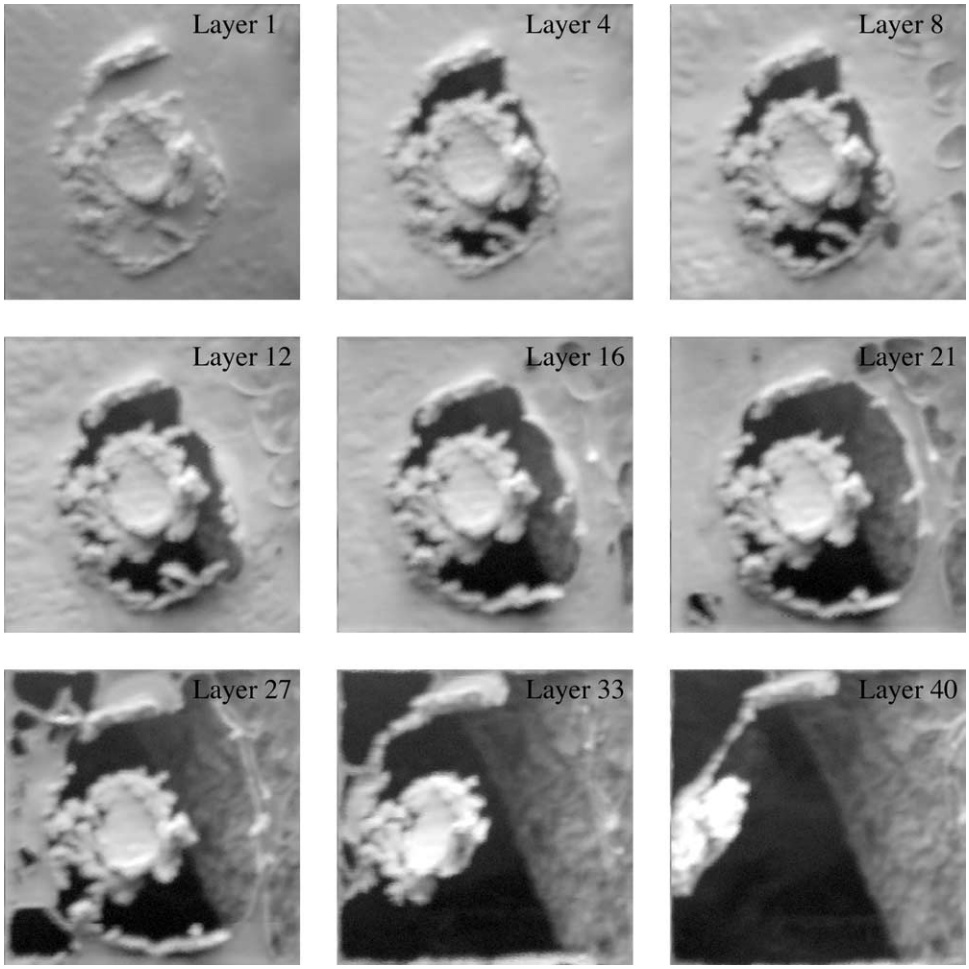

Fig. 3. Sequence of $10 \times 10\ \mu m^2$ SE images acquired during the measurement of a graphite section. The entire 40-layer measurement took 7.3 hours and the sequence was obtained with a 0.8 pA primary Cs^+ beam. Although the carbon film of the TEM grid begins to grow holes early in the measurement, the major part of the graphite slice remains suspended for a large part of the measurement, allowing meaningful isotopic data to be extracted from roughly the first 20 layers. Note that this extended sequence was acquired for demonstration purposes. In most analyses, the measurement would have been aborted after the sample support begins to fail.

$^{i}Ti/^{48}Ti$ for the analyzed areas were then calculated and normalized to those obtained on the perovskite standard. Results are expressed as δ-values, deviations of the measured ratios from the normal ratios in permil (‰).

Previous TEM studies (Croat et al., 2003) have shown that in many cases the elemental compositions (in particular the V content) of TiC crystals vary with their distance from the center of the graphite sphere. To investigate whether such a relationship also exists for their isotopic compositions, the relative locations of all analyzed TiC grains were determined from the images. This was done by determining the distance of the grain from the apparent center of the section and by calculating the distance of the given section from the three-dimensional center of the sphere by comparing the diameter of the slice with the diameter of the entire graphite spherule (i.e., 12 μm). Radial distances that were determined in this way are estimated to have an average error of ± 0.5 μm.

3. RESULTS

A typical NanoSIMS secondary electron image of one of the TEM sections is shown in Figure 1. The spatial resolution of this image is identical to that of the (unsmoothed) images of the simultaneously acquired C, N and/or O isotopes. These images, acquired with a Cs^+ primary beam, have sufficient spatial resolution to discern many of the internal features of this presolar graphite grain. In particular, some of the layers of turbostratic graphite (graphite with contorted lattice fringes and no long-range layer continuity) that have been observed in the TEM (Croat et al., 2003) can be seen in this slice, which appears compact in the center and less cohesive towards the outside. Since the TEM section shown here is from an off-center slice of the graphite, the diameter of this section is smaller than that of the whole spherule. Consequently, the centers of this and most other sections do not coincide with the three-dimensional center of the graphite grain.

Oxygen isotopes were measured in 9 microtome slices of particle KE3e#10. Due to the low abundance of ^{17}O, measurements of the $^{16}O/^{17}O$ ratio are subject to relatively large counting-statistical errors. The $^{16}O/^{17}O$ ratios of all analyzed slices were close to the terrestrial (SMOW) value of 2625 and showed little variation throughout the grain. In earlier 'bulk' measurements of this graphite particle the $^{16}O/^{17}O$ ratio was not deter-

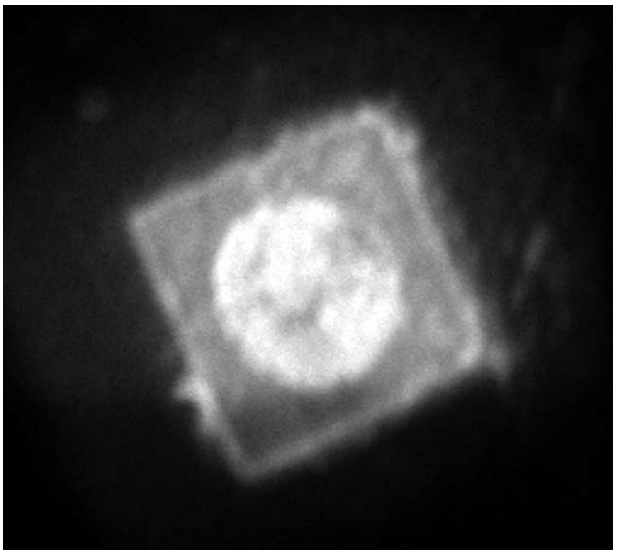

Fig. 4. Total (not mass-filtered) positive secondary ion image, obtained with an O^- primary ion beam, of a graphite slice that had previously been measured with a Cs^+ beam. The rectangular area imaged with the Cs^+ beam and the graphite slice are clearly visible, due to the signal from the previously implanted Cs. The area shown is 20 μm wide.

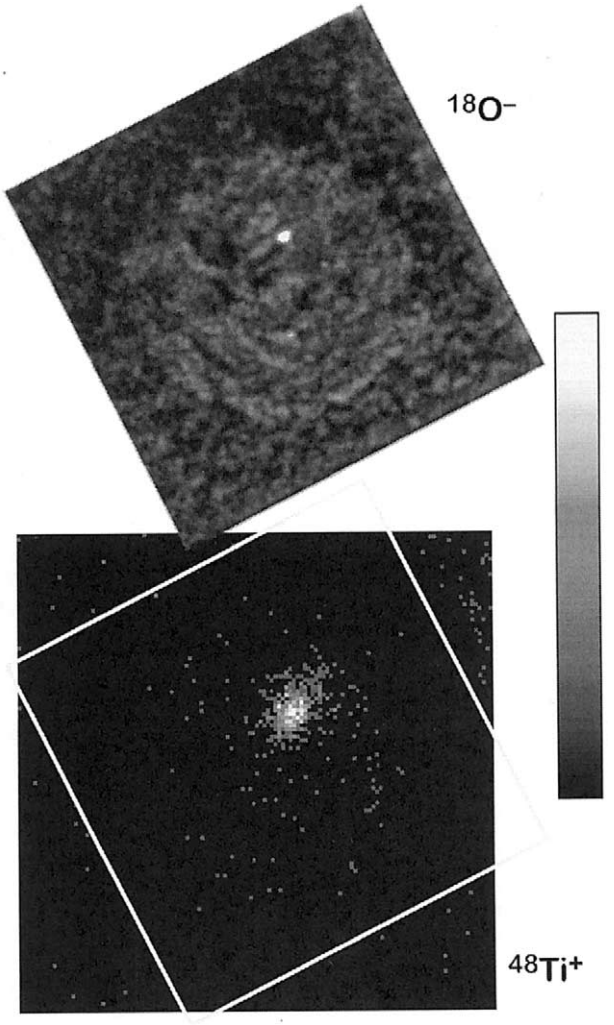

Fig. 5. Secondary ion raster images of $^{18}O^-$ (acquired with a Cs^+ primary beam) and $^{48}Ti^+$ (acquired with an O^- primary beam) from a TEM slice of presolar graphite KE3e#10. The sample was rotated between measurements and the ^{18}O raster area is indicated by the tilted square in the ^{48}Ti image. The diameter of the graphite grain (see top image) is 12 μm.

mined, but a terrestrial $^{16}O/^{17}O$ ratio is typical for other low-density graphite grains from the Murchison KE3 separate (Travaglio et al., 1999).

The determination of the $^{16}O/^{18}O$ ratios in the same TEM sections indicates large anomalies and a complex isotopic distribution. Figure 6 shows a representative false-color image of $^{16}O/^{18}O$ ratios in one microtome section of KE3e#10. The ratios vary from close to the terrestrial (SMOW) value of 499 to an ^{18}O-enriched value of around 200. Areas in gray did not yield a sufficiently high O signal for a statistically meaningful ratio determination. The $^{16}O/^{18}O$ ratio of the carbon film along the rim of the image shows some variability due to low count rates, but is on average terrestrial as expected. The isotopic composition of the graphite spherule itself is clearly distinct from that of the surrounding film. The most anomalous (i.e., the most ^{18}O-rich) area is found near the center of this slice and the $^{16}O/^{18}O$ ratios become more normal towards the rim of the particle. The average $^{16}O/^{18}O$ ratio of this spherule section is 345. This particular graphite section does not contain any internal subgrains.

We acquired C isotopic ratio images of all 11 graphite sections that were part of this study. A representative $^{12}C/^{13}C$ ratio image is shown in Figure 7. This image is of the same section as Figure 6; the C and O isotopic images were acquired in the same measurement. The area surrounding the graphite grain (i.e., the carbon film) has a normal (PDB) isotopic composition ($^{12}C/^{13}C = 89$). The graphite spherule is slightly ^{12}C enriched with $^{12}C/^{13}C$ ratios ranging up to around 130. As is the case with $^{16}O/^{18}O$, the areas with the most anomalous $^{12}C/^{13}C$ ratios are found near the center of the graphite grain, although the overall isotopic variations in C are not as prominent as in O. The average $^{12}C/^{13}C$ ratio of this section is 114, which is similar to the previously measured 'bulk' value of 125 $\pm$ 1 (Travaglio et al., 1999). The difference can be attributed to the sampling of different volumes, although there may also be some dilution with isotopically normal material in the TEM slices (see "Discussion").

To further investigate the isotopic gradients of $^{16}O/^{18}O$ and $^{12}C/^{13}C$ in the graphite, we have subdivided the data from one sample slice into subsets from five, roughly concentric regions as shown in the inset in Figure 8. These regions were visually defined based on what appeared to be the center of the slice in the secondary electron image. Region 1 is in the center of the particle and region 5 encompasses the outermost layers. Isotopic ratios of C and O were then calculated from the integrated counts in each region and the results are displayed in Figure 8. The error bars shown are 1 σ based on counting statistics only. As mentioned earlier, no significant isotopic variation can be seen in the $^{16}O/^{17}O$ ratio; the values for all regions are normal (i.e., $^{16}O/^{17}O = 2625$) within errors. However, monotonic gradients from center to rim are found in the $^{16}O/^{18}O$ and

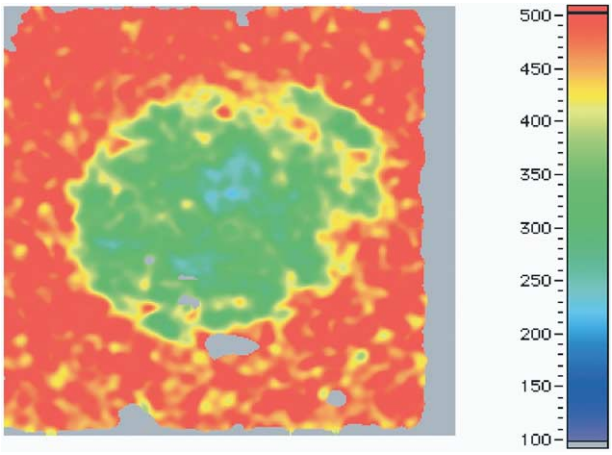

Fig. 6. False-color image of the O isotopic composition of one of the presolar graphite slices. The colors indicate varying $^{16}O/^{18}O$ ratios, ranging from around 200 in the center of the slice to the 'normal' ratio of 499 in the surrounding carbon film. The average $^{16}O/^{18}O$ ratio in this graphite section is 345. The apparent variations in the isotopic composition of the carbon film are due to counting statistics as a consequence of the lower total O counts in this area. In the gray areas the secondary O signal was too low for a meaningful determination of isotopic ratios. The area shown is 15 μm wide.

$^{12}C/^{13}C$ ratios with compositions becoming more 'normal' towards the surface of the grain.

We measured the N isotopes in only a single TEM section of this graphite spherule. There is no detectable radial gradient in the $^{14}N/^{15}N$ ratio and the average value for the entire slice is 256 $\pm$ 15, close to the normal (air) value of 272. No 'bulk' N isotopic composition for this graphite spherule is available from previous measurements, but other low-density graphites from the Murchison KE3 separate have N compositions that are compatible with that of this particle. The N isotopic composi-

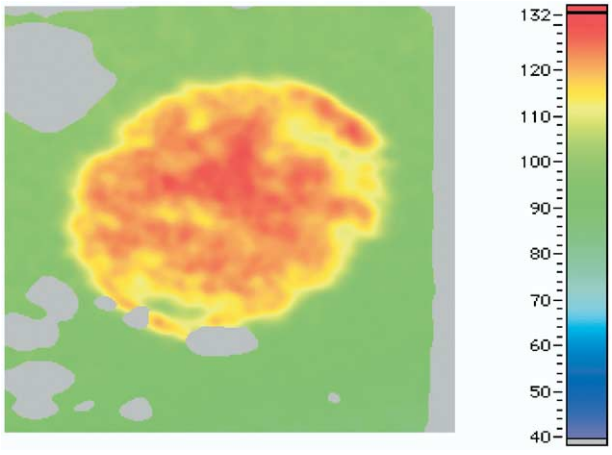

Fig. 7. False-color image of the C isotopic composition in the same slice as that shown in Figure 6. An average 'normal' $^{12}C/^{13}C$ ratio of 89 is measured in the surrounding carbon film and the highest ratio of around 130 is found near the center of the slice, while the average $^{12}C/^{13}C$ ratio of the entire slice is 114. In the gray areas the secondary ^{13}C signal was too low for a meaningful calculation of isotopic ratios. The area shown is 15 μm wide.

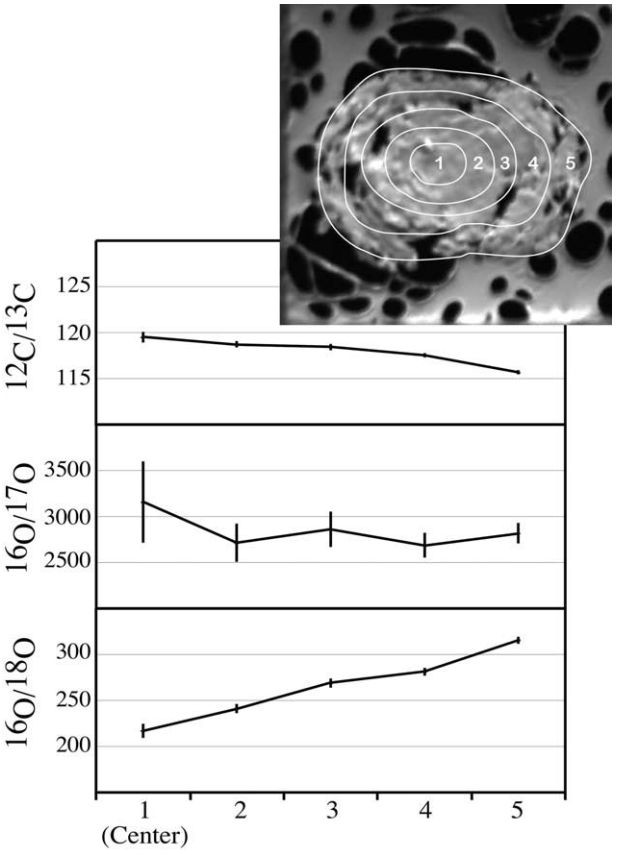

Fig. 8. Carbon and O isotopic compositions of different concentric regions in one of the graphite slices. The inset shows the regions for which average isotopic compositions have been calculated. The error bars shown are for 1-σ Poisson counting statistics. The $^{12}C/^{13}C$ and $^{16}O/^{18}O$ ratios are most anomalous in the center region and become more 'normal' towards the outside. Normal terrestrial isotopic ratios for $^{12}C/^{13}C$ and $^{16}O/^{18}O$ are 89 and 499, respectively. A similar gradient cannot be seen in the $^{16}O/^{17}O$ ratios, which are, within the much larger errors, compatible with the terrestrial value of 2625.

tions of many KE3 graphites cluster around the solar value, while others are ^{15}N-enriched by up to a factor of 10 (Travaglio et al., 1999).

There are internal TiC crystals in many of the TEM sections from graphite spherule KE3e#10 with sizes ranging from 15 to 500 nm (Croat et al., 2003). Figure 9 shows a TEM image of one section containing two such TiC subgrains. Since the negative secondary ion signal of Ti (with Cs^+ primary ions) is very low, we first tried to locate the TiC grains in the graphite section by monitoring the signal of $^{48}Ti^{12}C^-$ at mass 60. Despite the fact that we knew the exact locations of the TiC crystals from the TEM study, we did not detect a significant $^{48}Ti^{12}C^-$ signal in the area. To our surprise, however, both TiC grains are clearly visible as O-rich spots in the NanoSIMS image (Fig. 10). The large O^- secondary ion signal from the TiC grains allowed us to measure their O isotopic compositions without any significant contributions from the surrounding graphite matrix. Although the TiC grains make up only 0.1 vol.% of this graphite spherule (Croat et al., 2003), more than 5% of the secondary O signal came from these subgrains in some of the analyzed sections. In contrast, the TiC grains did not stand out in a similar way in the C^- images,

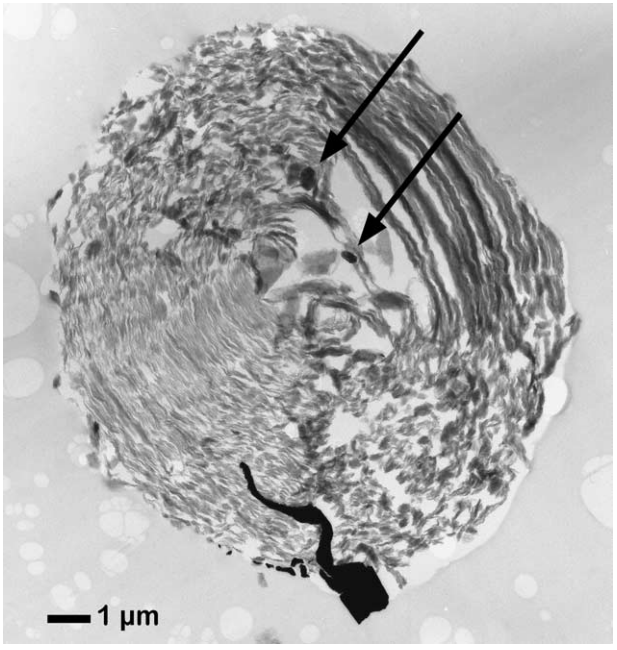

Fig. 9. TEM image (12 × 12 μm^2) of one of the graphite slices containing internal subgrains. The locations of two TiC crystals are indicated by the arrows.

indicating that their C^- secondary ion yield is comparable to that of the graphite.

To calculate the O isotopic compositions of the TiC crystals, small regions of interest were defined around the O-rich spots in the NanoSIMS images. Due to varying sizes of the TiC grains, possibly different O^- signals and slightly variable spatial resolutions in the images, it is difficult to adopt a uniform set of rules on how to define these regions of interest for different subgrains. Choosing extremely small regions results in low integrated counts and accompanying large statistical errors, while larger regions of interest may include unwanted contributions from the surrounding graphite matrix. We tried to balance these competing problems and believe that the calculated O isotopic ratios are representative for the TiC crystals with only minor contributions from the graphite. The same may not be true for the calculated C isotopic compositions. Because the C signal from the TiC is no higher than that from the surrounding graphite matrix, the C isotopic ratios of the TiC grains are probably strongly affected by the composition of the surrounding matrix. The high O^- secondary ion signals from the TiC crystals makes it necessary to check the data for potential distortions due to the recently described QSA effect (Slodzian et al., 2001). This effect can lead to an undercounting of the most abundant isotope due to quasi-simultaneous arrival of two or more secondary ions at the same detector. In this case, however, we are confident that any possible effect on the isotopic ratios reported here is negligible within the given errors. The spatial resolution of the ion images is insufficient to distinguish between contributions from the center and the surface (rim) of individual TiC crystals.

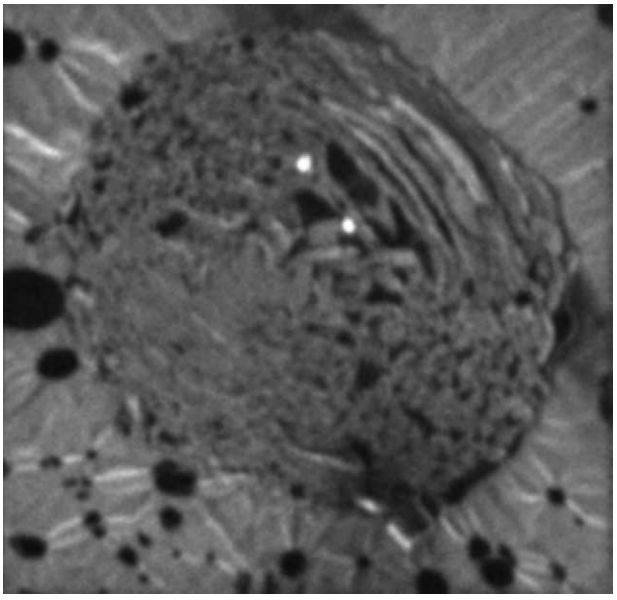

Fig. 10. NanoSIMS $^{16}O^-$ image (12 × 12 μm^2) of the same slice as shown in the TEM image in Figure 9. Many details from the TEM image can be identified in the NanoSIMS image and the two TiC grains are clearly visible due to their high O signal.

Oxygen and C isotopic data for a total of 11 individual TiC grains were obtained from the images of presolar graphite KE3e#10, and the O data are shown in Table 1 and Figure 11. The $^{16}O/^{18}O$ ratios of the TiC grains within this graphite vary from 14 to 250, while all calculated $^{16}O/^{17}O$ ratios are close to normal. The 'bulk' O isotopic composition of KE3e#10, as determined with the ims3f instrument before slicing of this spherule, and the composition of inclusion-free areas of the graphite in the NanoSIMS measurements are shown as well. No effort was made to determine an average O isotopic composition of the inclusion-free areas of the graphite, which would be complicated by the internal isotopic gradient, the different locations of the slices in the original spherule, and the varying degrees of physical fragmentation of the sections along their rims. However, the $^{16}O/^{18}O$ ratios of randomly selected areas of inclusion-free graphite vary from 220 to 390. This range is far smaller than the variation in the O isotopic compositions of the TiC subgrains. Also shown in Figure 11 are 'bulk' O isotopic compositions of other low-density presolar graphite grains (Travaglio et al., 1999) for comparison.

Since previous studies (Croat et al., 2003) found that the V/Ti ratios of the internal TiC in some cases (although not strongly in KE3e#10) vary with their location within the graphite, we investigated whether such a relationship exists with respect to their $^{16}O/^{18}O$ ratios. Figure 12 shows a plot of $^{16}O/^{18}O$ ratios vs. the distance from the center of the sphere for all 11 studied TiC crystals. While there is a large range of $^{16}O/^{18}O$ ratios in TiC grains with approximately the same radial distance from the center, the data do not span a large enough range in radial distance to determine whether there is a correlation.

The calculated C isotopic compositions of the TiC crystals were in all cases indistinguishable from those of the immediately surrounding graphite matrix (e.g., a TiC crystal appears to have a $^{12}C/^{13}C$ ratio of 120 if the surrounding graphite has that composition). As discussed above, this could be due to mixing

Table 1. Ti and O isotopic compositions of internal TiC crystals.

Name	Distance	$^{16}O/^{18}O$	$^{16}O/^{17}O$	$\delta^{46}Ti/^{48}Ti$	$\delta^{47}Ti/^{48}Ti$	$\delta^{49}Ti/^{48}Ti$	$\delta^{50}Ti/^{48}Ti$
KE3E#10 B2T1	2.2 μm	14 ± 1	3330 ± 420	n. d.	n. d.	n. d.	n. d.
KE3E#10 B2T2	2.3 μm	250 ± 9	2210 ± 240	n. d.	n. d.	n. d.	n. d.
KE3E#10 B2T4	2.8 μm	63 ± 2	2540 ± 370	n. d.	n. d.	n. d.	n. d.
KE3E#10 B3T1	3.2 μm	64 ± 6	3060 ± 1100	n. d.	n. d.	n. d.	n. d.
KE3E#10 B3T2	5.0 μm	155 ± 12	3160 ± 1010	n. d.	n. d.	n. d.	n. d.
KE3E#10 B3T5	3.2 μm	245 ± 14	2400 ± 410	n. d.	n. d.	n. d.	n. d.
KE3E#10 B5T1	3.1 μm	106 ± 4	2640 ± 950	−56 ± 10	−61 ± 11	538 ± 10	36 ± 12
KE3E#10 B6T1	4.4 μm	91 ± 2	2060 ± 330	n. d.	n. d.	n. d.	n. d.
KE3E#10 B6T2	5.1 μm	154 ± 6	2470 ± 590	−86 ± 12	−61 ± 13	507 ± 12	37 ± 15
KE3E#10 B6T3	3.3 μm	114 ± 5	2410 ± 610	n. d.	n. d.	n. d.	n. d.
KE3E#10 B6T4	2.7 μm	42 ± 1	3500 ± 540	−35 ± 12	−67 ± 12	511 ± 12	29 ± 14
KE3E#10 'Bulk'	n/a	174 ± 7	n. d.	44 ± 35	−53 ± 33	440 ± 53	10 ± 53

Errors are 1 σ based on counting statistics.

of secondary ion signals from both areas as long as the intrinsic C isotopic compositions of the subgrains are not extremely different from that of the graphite. In other words, the C isotopic compositions of the TiC crystals might only appear to be similar to those of the graphite. It might be possible to further quantify this statement by determining the secondary ion signals of graphite and TiC standards, but that is beyond the scope of this study.

Finally, we measured the Ti isotopic compositions of 3 TiC crystals of which there was still sufficient material left after the C and O imaging measurements. These TiC crystals come from graphite sections located on the top of one of the copper bars of the TEM grid (see earlier discussion). NanoSIMS images from the measurement of TiC "KE3E#10 B5T1" are shown in Figure 5. Despite the fact that these subgrains had been partially consumed during the previous C-O isotopic measurements, they still yielded between 70,000 and 102,000 cumulative counts of ^{48}Ti. The results of

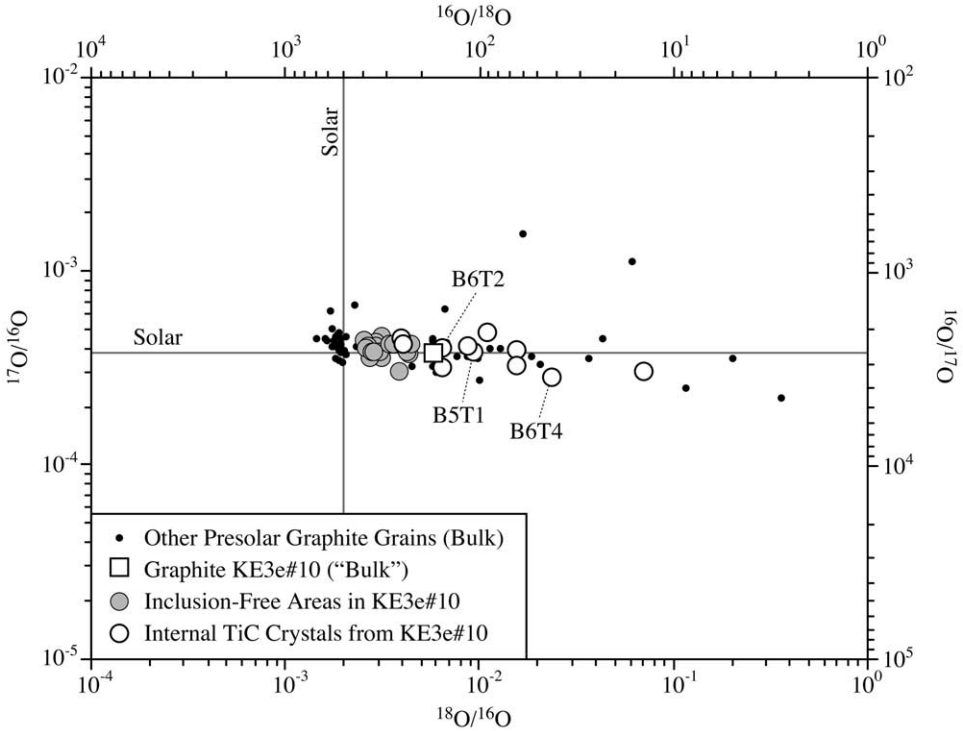

Fig. 11. Three-isotope plot of the O isotopic compositions of components of KE3e#10 and of bulk ratios of other presolar graphite grains. The 'bulk' $^{16}O/^{18}O$ value for the entire graphite spherule, measured previously with the ims3f ion microprobe, falls in the middle of the distribution measured in other presolar graphites (Travaglio et al., 1999), making KE3e#10 a 'typical' particle with respect to its $^{18}O/^{16}O$ ratio. A 'bulk' value for $^{17}O/^{16}O$ has not been determined and for the purpose of this plot, a solar ratio is assumed. Examination of the isotopic compositions of the subcomponents reveals that the inclusion-free areas of the graphite are much closer to the solar value ($^{18}O/^{16}O = 2.004 \times 10^{-3}$) than the 'bulk', which is dominated by large ^{18}O contributions from the internal TiC crystals. The three individually labeled points B5T1, B6T2 and B6T4 represent those TiC particles whose Ti isotopic compositions have also been measured.

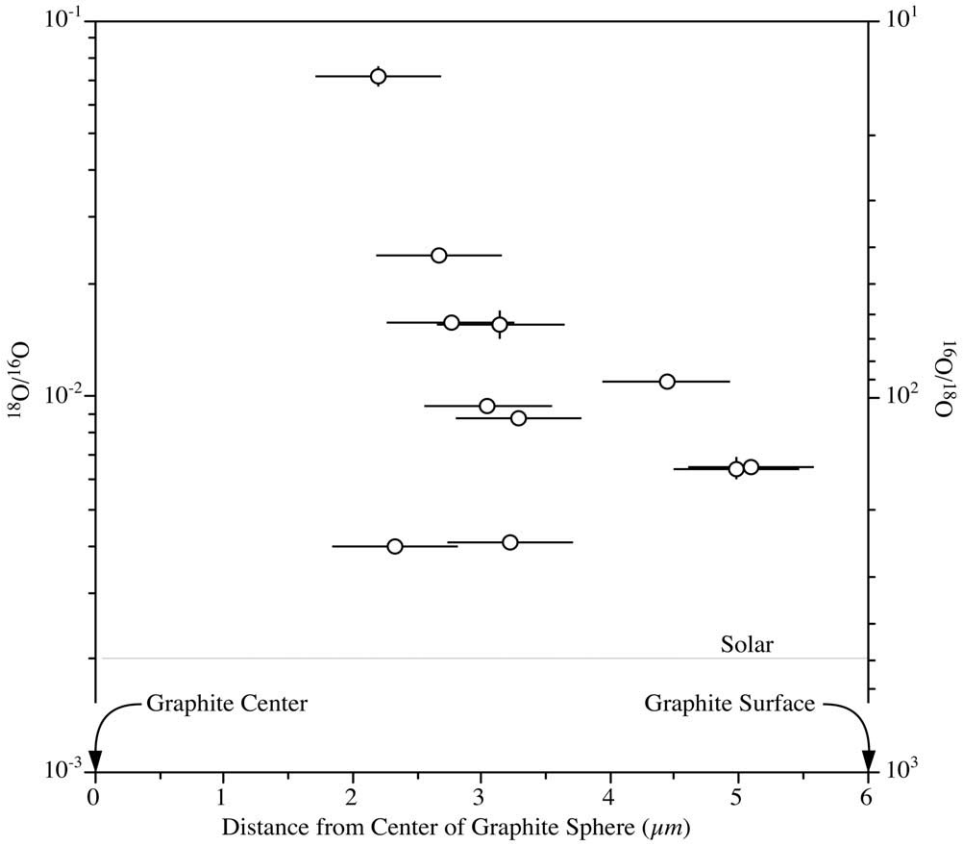

Fig. 12. Diagram of the $^{18}O/^{16}O$ ratios in individual TiC crystals plotted against their distance from the center of the graphite spherule. See text for discussion.

the Ti isotopic measurements are given in Table 1 and shown in Figure 13, together with the previously determined 'bulk' values. The δ-value of ^{48}Ti is zero by definition. The Ti isotopic compositions of all three analyzed TiC crystal are identical within errors and are close to the 'bulk' composition.

Together with the Ti isotopes, we also recorded the count rates of ^{40}Ca, ^{43}Ca, and ^{44}Ca in the three TiC grains. Due to the low count rates, the precision of these measurements is limited. All $^{43}Ca/^{40}Ca$ and two $^{44}Ca/^{40}Ca$ ratios in these subgrains are normal within Poisson errors. The only exception is "KE3E#10 B5T1," which shows a $^{44}Ca/^{40}Ca$ excess of (219 ± 55) ‰. Under the assumption that the excess is due to in situ decay of ^{44}Ti (Nittler et al., 1996), we infer an initial $^{44}Ti/^{48}Ti$ ratio of 0.00011 ± 0.00003 for this TiC grain. A relative Ti/Ca sensitivity factor of 0.18 was determined from the measurements of the perovskite standard and this value is identical to the one used in previous studies (Hoppe et al., 2000).

4. DISCUSSION

The submicrometer-scale measurements of the internal isotopic structure of the presolar graphite grain reported here represent a significant advance over previous 'bulk' isotopic measurements. These data give a unique view of the origin and history of this particle and its numerous internal grains. Moreover, such observations of the radial isotopic composition of

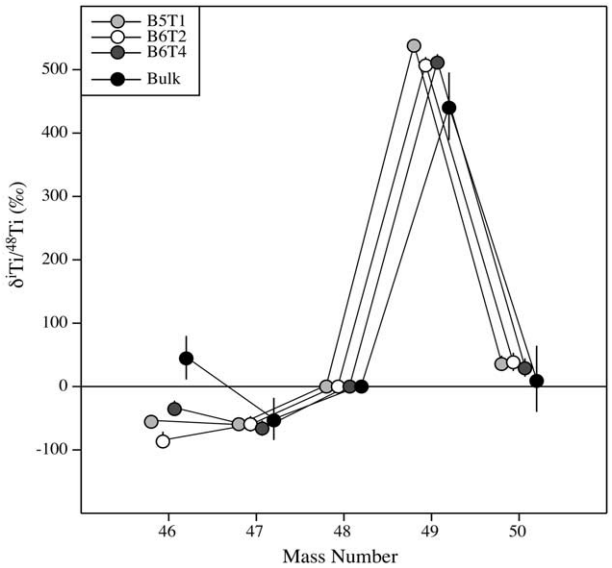

Fig. 13. Plot of the Ti isotopic compositions of the presolar graphite grain KE3e#10 and of three internal TiC grains. The 'bulk' value was measured with the ims3f ion microprobe and the composition of three individual TiC subgrains was determined with the NanoSIMS. Note that the errors are smaller for the NanoSIMS measurement of individual TiC grains than for the previous 'bulk' measurement with the ims3f. The patterns are slightly offset horizontally to not obscure the error bars.

the grain and its TiC inclusions raise the possibility of discerning the degree of large-scale mixing of material in the supernova ejecta from which it formed.

Overall, there is good agreement of the new NanoSIMS data with the 'bulk' measurements made with the ims3f ion microprobe, whenever such a comparison could be made. In cases where there are small differences, they can in most cases be explained by the fact that the ims3f measurements do not truly sample the bulk spherule, but represent merely an average composition of a subvolume of the particle. It is commonly assumed that the subvolume consumed during 'bulk' measurements is representative of the whole spherule but, given the isotopic heterogeneities revealed in our present study, this assumption is not necessarily correct. The fraction of the particle that was analyzed in the ims3f was necessarily consumed and the following TEM and NanoSIMS studies were performed on the remainder. Although these particles appear to have a high degree of azimuthal compositional symmetry at a given radius (Zinner et al., 1995; Croat et al., 2003), we do not know how much of the graphite was consumed during the 'bulk' analysis. Another reason for small differences between 'bulk' and NanoSIMS results may be the sample mounting. For the original ims3f 'bulk' measurements the graphite spherule was mounted on a Au substrate, whereas it was embedded in resin and sliced for the TEM and NanoSIMS work. Although the spatial resolution of the NanoSIMS makes it possible to distinguish different phases in most cases, it cannot be ruled out that minor contributions from the resin led to a slight contamination of the graphite with isotopically normal C and O.

'Bulk' SIMS analyses of low-density graphite spherules sometimes show gradually changing isotopic ratios during the course of a measurement, which is seen as an indication for the presence of radial isotopic gradients in these particles (Zinner et al., 1995; Travaglio et al., 1999). Those measurements, however, do not allow a determination of the true ratios in the core of the particle, since the secondary ion signal from the core region is mixed with that of much larger areas from the outer regions. The substantially improved spatial resolution of the NanoSIMS has enabled us to obtain a far more detailed view of the radial isotopic distribution within these grains. The observed isotopic gradients are not correlated with the distances to the nearest 'gap' in the graphite or with the number of gaps in different parts of the graphite. There are two possible explanations for the presence of gradients. One is that the radially changing isotopic ratios reflect a temporal change in the surrounding gas during the original growth of the spherule. This explanation is appealing because it would give detailed constraints on the isotopic evolution of the environment in which the graphite particles were growing, a process which can take up to several years for graphite spheres of this size (Bernatowicz et al., 1996). However, all isotopic gradients observed in this study are towards a more 'normal' composition at the outer regions of the particle, raising the possibility that the gradients resulted from exchange with an isotopically normal reservoir. Such an exchange would be less efficient in the center of the particle, leaving the core with an isotopic composition that is closest to the original one. As a consequence, the isotopic composition of the core can only be seen as a lower limit to the original isotopic anomaly. The isotopically normal reservoir with which the graphite interacted could be the laboratory during the chemical processing that led to the isolation of the graphite grains, the meteorite matrix, the presolar gas cloud, or a combination of these. Detailed isotopic measurements of presolar graphite in situ could possibly narrow down this list.

One of the exciting results of this study is the isotopic analysis of submicrometer sized "interstellar grains within interstellar grains" (Bernatowicz et al., 1991). Locating TiC crystals and measuring their O isotopic compositions turned out to be easier than expected due to the surprisingly high O^- secondary ion signal from the TiC subgrains (Fig. 10). It is not immediately clear why we obtain such a high O signal from these particles or in what form the O is present in the TiC. Secondary ion signals in SIMS are subject to various matrix, phase boundary, implantation, and morphology effects, which makes it impossible to directly quantify elemental abundances without detailed knowledge of the sample and the sputtering conditions. EDXS measurements of TiC subgrains in the TEM found O generally to be present only in trace concentrations (O/C count ratios from 0.01 to 0.1). This O content is within errors the same as that seen in the surrounding graphite. However, due to significant peak overlap at low energies in the TiC spectra, these values are quite uncertain. The use of improved EDXS standards and energy loss electron spectrometry are planned to clarify the O content of the TiC grains. The high O signal seen in the NanoSIMS images is likely due to enhancement by the implantation of Cs from the primary Cs^+ ion beam during the measurement. The implanted Cs concentration is higher in TiC than in the graphite and implanted Cs is known to significantly enhance the signal of negative secondary ions. Some TiC crystals have 3–15 nm thick amorphous (Croat et al., 2003) or partially amorphous (Bernatowicz et al., 1999) rims, but based on the available data it is not clear whether these rims contain the high O concentrations. Overall, KE3e#10 does not contain a higher percentage of rimmed TiC grains than other graphites from KE3 (Croat et al., 2003). Thus, it is not clear in what form the O is associated with the TiC crystals and whether it was acquired during the growth of the TiC crystals or is the result of surface reactions on the TiC before they were embedded into the growing graphite spherule. In future studies we will attempt to further improve the spatial resolution of the NanoSIMS imaging measurements to address these questions.

The distribution of O isotopic compositions in the different components of the presolar graphite KE3e#10 (Fig. 11) clearly shows that most of the ^{18}O-enrichment is carried by the TiC crystals and not by the graphite itself. The 'bulk' O isotopic composition, consequently, is a combination of contributions from both components. However, due to the possibility of different degrees of secondary ion signal enhancement discussed above, this combination *does not* necessarily represent the average isotopic composition of all O within the entire graphite spherule. Since both NanoSIMS and ims3f SIMS measurements were made with a Cs^+ primary ion beam and negative secondary ions, results from both instruments are similarly affected.

Figure 11 also shows O isotopic compositions in other low-density presolar graphite grains (Travaglio et al., 1999). The compositions of all individually measured components of KE3e#10 cover a range similar to that of the observed 'bulk' values, raising the possibility that the variability of 'bulk' compositions in presolar graphite grains is simply the result of varying

concentrations of internal TiC crystals. However, no such simple correlation between the overall TiC abundance in a particular graphite and its 'bulk' deviation of $^{16}O/^{18}O$ from solar was found in a recent TEM study of KE3 graphites (Croat et al., 2003).

As discussed earlier, the original O isotopic composition of the graphite matrix itself may have been more ^{18}O-rich than what is measured now, possibly even as anomalous as the most anomalous ^{18}O-rich subgrains. The TiC crystals may also have experienced, although to a lower degree, the isotopic exchange leading to more normal O isotopic compositions. To investigate this possibility further, we looked at the distribution of $^{16}O/^{18}O$ isotopic ratios in the analyzed TiC crystals as a function of their physical location inside the graphite spherule (Fig. 12). If all TiC grains started out with the same, ^{18}O-rich composition and the sole mechanism for the varying isotopic compositions of the TiC grains was isotopic exchange, we would expect a radial gradient, similar to what is observed for the graphite matrix. The number of data points in Figure 12 is limited, but it is obvious that no such simple trend exists. For most of the TiC grains that were analyzed in the NanoSIMS, we do not have direct size information from the TEM study. Therefore, it is not clear whether there is a correlation between the size and the isotopic composition of the TiC grains.

Isotopic abundances of Ti were only measured in 3 TiC subgrains and their ratios turned out to be identical within errors and close to the previously determined 'bulk' values (Travaglio et al., 1999), which had larger uncertainties (Fig. 13). There is no evidence for isotopic exchange of Ti isotopes and virtually all Ti in the graphite sections comes from the TiC crystals (cf. Fig. 5). Enrichments of ^{49}Ti in SiC X-grains were found to be due to in situ decay of ^{49}V, as indicated by a positive correlation between $^{49}Ti/^{48}Ti$ and $^{51}V/^{48}Ti$ in those supernova grains (Hoppe and Besmehn, 2002). An analogous origin of the ^{49}Ti enrichments in TiC is likely and further studies will, therefore, include correlated V/Ti and $^{49}Ti/^{48}Ti$ measurements. Since ^{49}V has a half life of 330 days, the detection of the decay product ^{49}Ti in TiC grains would put time constraints on the formation of the TiC grains after the supernova explosion. If we assume that indeed all TiC grains in the spherule KE3e#10 have identical Ti isotopic compositions and that the O in the TiC is the result of a reaction with a gas before they were incorporated into the graphite (Croat et al., 2003), we are faced with an interesting conundrum. It would imply that the TiC crystals were formed in an environment with uniform Ti isotopic composition in the ejecta of the supernova, were then exposed to environments with distinctly different $^{18}O/^{16}O$ ratios, and were finally incorporated into the same graphite spherule. However, we currently have only limited statistics and it remains to be seen whether homogeneous Ti isotopic compositions in different TiC subgrains are commonplace in other low-density graphites.

The observation of evidence for extinct ^{44}Ti (Nittler et al., 1996) in one of the TiC crystals is not surprising, because virtually all Ti in the spherules comes from the embedded subgrains, and such excesses in ^{44}Ca are frequently found in 'bulk' measurements of low-density graphites most of which appear to originate in supernovae (Nittler et al., 1996). Previous 'bulk' measurements in this particular graphite spherule, however, did not show any ^{44}Ca excesses (Travaglio et al., 1999). That result is consistent with the measurements presented here, where a relatively low initial $^{44}Ti/^{48}Ti$ of 0.00011 was observed in only one of three TiC subgrains. The presence of short-lived ^{44}Ti confirms the previous identification of KE3e#10 (on the basis of its O isotopic composition) as a supernova condensate (Croat et al., 2003).

The Si isotopic composition, $\delta^{29}Si/^{28}Si = (-85 \pm 31)$ ‰, $\delta^{30}Si/^{28}Si = (-123 \pm 30)$ ‰, of this graphite grain has been determined in previous 'bulk' measurements (Travaglio et al., 1999). Such ^{28}Si excesses in combination with evidence for ^{44}Ti are found in many SiC X-grains and low-density graphites. However, both the ^{28}Si excess in the 'bulk' graphite KE3E#10 and the inferred $^{44}Ti/^{48}Ti$ ratio in the TiC subgrain B5T1 are significantly smaller than in other, previously measured supernova grains with such anomalies (Nittler et al., 1996; Hoppe et al., 2000; Besmehn and Hoppe, 2003). That both of these isotopic effects are smaller is consistent with the previously reported negative correlation between $\delta^{29}Si/^{28}Si$ and $^{44}Ti/^{48}Ti$ (Nittler et al., 1996; Hoppe et al., 2000), which indicates that ^{28}Si and ^{44}Ti are produced together. This isotopic signature originates in the innermost layers of a supernova (Woosley and Weaver, 1995) and material from there must have mixed with material from the C-rich outer zones for graphite to form (Bernatowicz et al., 1996). In this NanoSIMS study we did not look at the isotopic composition or spatial distribution of Si. Previous SIMS depth profile measurements in 'bulk' graphites had indicated that both Si and O are distributed more or less homogeneously throughout the graphite (Travaglio et al., 1999), but at least for O this is not always the case, as demonstrated in this study.

5. CONCLUSIONS

We looked at the composition of a single presolar graphite grain and used NanoSIMS elemental and isotopic imaging to directly measure properties such as isotopic gradients and heterogeneous elemental distributions that previously could only be *inferred*. We found a significant difference between the O isotopic compositions of the graphite matrix and the embedded TiC crystals, with the latter being extremely ^{18}O-rich. This implies that so-called 'bulk' O isotopic compositions of presolar graphites do not represent the average composition of all O within the spherule, if we assume that the relative O secondary ion yields are different in graphite and TiC. There also is large variability of O isotopic compositions among the TiC crystals, which is in stark contrast to their uniform Ti isotopic compositions. Such observations, together with structural and mineralogical studies (Croat et al., 2003) offer additional parameters for the understanding of grain formation in supernova ejecta. The combination of TEM and NanoSIMS measurements makes it possible to look at the isotopic makeup of submicrometer phases with unprecedented detail. We will continue this multitechnique approach and extend studies of this kind to a larger number of presolar grains and to other isotopic systems. This will allow us to take a broader look at the distribution of isotopic compositions in low-density presolar graphites and to compare the results with proposed supernova mixing models for the creation of such grains.

Acknowledgments—This work was made possible by NASA grants NAG5-11865 and NAG5-10426 (NNG04GG13G). We would like to

thank reviewers P. Hoppe and G. Huss for their helpful comments and an anonymous reviewer for the best review ever received (FJS).

Associate editor: U. Ott

REFERENCES

Amari S., Anders E., Virag A. and Zinner E. (1990) Interstellar graphite in meteorites. *Nature* **345,** 238–240.

Amari S., Lewis R. S. and Anders E. (1994) Interstellar grains in meteorites: I. Isolation of SiC, graphite and diamond; size distributions of SiC and graphite. *Geochim. Cosmochim. Acta* **58,** 459–470.

Amari S., Zinner E. and Lewis R. S. (1995) Large ^{18}O excesses in circumstellar graphite grains from the Murchison meteorite: Indication of a massive-star origin. *Astrophys. J.* **447,** L147–L150.

Amari S., Zinner E. and Lewis R. S. (1996) ^{41}Ca in presolar graphite of supernova origin. *Astrophys. J.* **470,** L101–L104.

Bernatowicz T., Bradley J., Amari S., Messenger S. and Lewis R. (1999) New kinds of massive star condensates in a presolar graphite from Murchison. *Lunar Planet. Sci.* **XXX,** Abstract #1392.

Bernatowicz T. J., Amari S., Zinner E. K. and Lewis R. S. (1991) Interstellar grains within interstellar grains. *Astrophys. J.* **373,** L73–L76.

Bernatowicz T. J., Cowsik R., Gibbons P. C., Lodders K., Fegley B. Jr., Amari S. and Lewis R. S. (1996) Constraints on stellar grain formation from presolar graphite in the Murchison meteorite. *Astrophys. J.* **472,** 760–782.

Bernatowicz T. J. and Zinner E (1997) Astrophysical Implications of the Laboratory Study of Presolar Materials. *AIP Conf. Proc.* **402,** 750 pp.

Besmehn A. and Hoppe P. (2003) A NanoSIMS study of Si- and Ca-Ti-isotopic compositions of presolar silicon carbide grains from supernovae. *Geochim. Cosmochim. Acta* **67,** 4693–4703.

Croat T. K., Bernatowicz T., Amari S., Messenger S. and Stadermann F. J. (2003) Structural, chemical and isotopic microanalytical investigations of graphite from supernovae. *Geochim. Cosmochim. Acta* **67,** 4705–4725.

Hillion F., Horreard F. and Stadermann F. J (1999) Recent results and developments on the CAMECA NanoSIMS 50. *12th International Conference on Secondary Ion Mass Spectrometry,* 209–212.

Hoppe P., Amari S., Zinner E. and Lewis R. S. (1995) Isotopic compositions of C, N, O, Mg, and Si, trace element abundances and morphologies of single circumstellar graphite grains in four density fractions from the Murchison meteorite. *Geochim. Cosmochim. Acta* **59,** 4029–4056.

Hoppe P. and Besmehn A. (2002) Evidence for extinct vanadium-49 in presolar silicon carbide grains from supernovae. *Astrophys. J.* **576,** L69–L72.

Hoppe P., Strebel R., Eberhardt P., Amari S. and Lewis R. S. (2000) Isotopic properties of silicon carbide X grains from the Murchison meteorite in the size range 0.5–1.5μm. *Meteorit. Planet. Sci.* **35,** 1157–1176.

Huss G. R. and Lewis R. S. (1995) Presolar diamond, SiC and graphite in primitive chondrites: Abundances as a function of meteorite class and petrologic type. *Geochim. Cosmochim. Acta* **59,** 115–160.

Nittler L. R. (2003) Presolar stardust in meteorites: recent advances and scientific frontiers. *Earth Planet. Sci. Lett.* **209,** 259–273.

Nittler L. R., Amari S., Zinner E., Woosley S. E. and Lewis R. S. (1996) Extinct ^{44}Ti in presolar graphite and SiC: Proof of a supernova origin. *Astrophys. J.* **462,** L31–L34.

Slodzian G., Chaintreau M., Dennebouy R. and Rousse A. (2001) Precise in situ measurements of isotopic abundances with pulse counting of sputtered ions. *Eur. Phys. J. Appl. Phys.* **14** (*3*), 199–231.

Stadermann F. J., Walker R. M. and Zinner E. (1999) Sub-micron isotopic measurements with the CAMECA NanoSIMS. *Lunar Planet. Sci.* **XXX,** Abstract #1407.

Travaglio C., Gallino R., Amari S., Zinner E., Woosley S. and Lewis R. S. (1999) Low-density graphite grains and mixing in type II supernovae. *Astrophys. J.* **510,** 325–354.

Woosley S. E. and Weaver T. A. (1995) The evolution and explosion of massive stars, II. Explosive hydrodynamics and nucleosynthesis. *Astrophys. J. Suppl.* **101,** 181–235.

Zinner E. (1997) Presolar Material in Meteorites: an Overview. In *Astrophysical Implications of the Laboratory Study of Presolar Materials* (ed. T. J. Bernatowicz and E. Zinner), pp. 3–26. AIP.

Zinner E. (1998) Stellar nucleosynthesis and the isotopic composition of presolar grains from primitive meteorites. *Ann. Rev. Earth Planet. Sci.* **26,** 147–188.

Zinner E., Amari S., Wopenka B. and Lewis R. S. (1995) Interstellar graphite in meteorites: Isotopic compositions and structural properties of single graphite grains from Murchison. *Meteoritics* **30,** 209–226.